

The exact Maxwell evolution equation of resonators dynamics: the temporal coupled-mode theory revisited

T. Wu,¹ and P. Lalanne^{1*}

¹ Laboratoire Photonique, Numérique et Nanosciences (LP2N), IOGS- Université de Bordeaux-CNRS, 33400 Talence cedex, France

* philippe.lalanne@institutoptique.fr

Abstract. Despite its widespread significance, the temporal coupled-mode theory (CMT) lacks a foundational validation based on electromagnetic principles and stands as a phenomenological theory relying on fitted coupling coefficients. We employ an ab initio Maxwellian approach using quasinormal-mode theory to derive an "exact" Maxwell evolution (EME) equation for resonator dynamics. While the resulting differential equation bears resemblance to the classical one, it introduces novel terms embodying distinct physics, suggesting that the CMT predictions could be faulted by dedicated experiments, for instance carried out with short pulses or resonators of sizes comparable to or greater than the wavelength. Nonetheless, our examination indicates that, despite its inherent lack of strictness, the CMT enables precise predictions for numerous nanophotonics-related experiments due to the flexibility provided by the fitted coupling coefficients. The new EME equation is anticipated to be applicable to all electromagnetic resonator geometries, and the theoretical approach we have taken can be extended to other wave physics.

Keywords: coupled-mode theory, quasinormal mode, dissipative coupling, non-Hermitian physics, electromagnetic resonators.

1. Introduction

The temporal coupled-mode theory (CMT) is an acclaimed and widely used theoretical framework for modeling the continuous wave response and temporal dynamics of any integrated or free-space photonic resonant structure. Initially developed for the analysis and design of resonant systems, as well as the comprehension of energy coupling into and out of cavities and its exchange among various resonant modes [1-4], CMT has evolved over three decades to encompass advanced systems and contemporary physical phenomena. These include noninstantaneous nonlinearities, gain, PT-symmetry, 2D photonic materials, and time-reversal, underscoring its vast capabilities.

CMT holds the potential to simplify the description of resonant systems with arbitrary material compositions and geometric configurations. Even intricate systems can be treated as lumped harmonic oscillators. At its core, the dynamics of the resonator can be reduced to an ordinary differential equation with respect to time

$$\frac{da_m}{dt} = -i\tilde{\omega}_m a_m + \langle \kappa_m^* | s_+ \rangle, \quad (1)$$

where $|a_m|^2$ represents the energy stored in the m^{th} mode of the resonator and $\tilde{\omega}_m$ is the complex-valued frequency of the mode, encompassing radiative decay to excitation channels, free space and absorption. We intentionally use conventional notations in Eq. (1) and denote by $|s_+\rangle$ the vector of input amplitudes and $|\kappa_m\rangle$ the vector of coupling constants between the mode and the channels.

The evolution equation (1) is typically accompanied by an additional linear equation that delineates the decay of the resonator into each individual channel. Generally, the coupling coefficients introduced by these additional equations are derived with multiple smart assumptions. We will not delve into them here, maintaining our focus on the fundamental dynamics of the resonator.

Equation (1) stands as a pivotal outcome of CMT, offering high intuitiveness, computational simplicity, and a clear delineation of the physics governing resonances. However, it should be regarded as heuristic, lacking theoretical support for its validity. In standard usage, physical quantities characterizing the cavity (e.g., resonance frequency and coupling constants) are fitted, and

their extraction is generally believed to be rigorously feasible through numerical or experimental means.

The primary motivation behind this work was to establish a rigorous foundation for Eq. (1) and derive an analytical expression for it directly from Maxwell equations. In this pursuit, we discovered that the evolution equation is only an approximation. Our objectives are thus to elucidate the approximations inherent in the CMT model, comprehend their consequences, and raise awareness when the differences become consequential. We contend that the approximations are significant enough to warrant a dedicated publication, building upon an analysis initially presented in a prior publication [5] by the same group.

Except for the study in [6], as far as we are aware, there is a lack of any Maxwellian derivation of the CMT in the existing literature. Furthermore, based on our comprehension of the analysis in [6], it appears that the Maxwellian evolution equation derived in our current work differs from that derived in [6]. Also, regarding the accuracy of the CMT evolution equation under specific conditions also vary.

In Section 2, we initiate our exploration from Maxwell equations, undertaking an ab-initio derivation of the differential equation governing the dynamics of resonators. This derivation leads us to an equation distinct from Eq. (1), which we shall refer to as the “exact” Maxwell evolution (EME) equation. The ability to derive this is facilitated by the advancements achieved over the past decade in electromagnetic quasinormal modes (QNMs) [7].

In Section 3, we highlight the two primary distinctions between the CMT evolution equation and the EME equation: the coupling coefficient is non-local, and the excitation is not directly proportional to the driving field, but to its temporal derivative. We also conduct a comprehensive assessment through a generic example, enabling us to discern the circumstances under which the predictions of the CMT and EME equations significantly differ.

The insights gleaned from our conclusions in the realm of electromagnetism hold the potential to extend their influence to other types of waves for which QNM theory offers robust support [8].

2. The exact Maxwell evolution equation

The EME equation is derived by employing electromagnetic quasinormal mode (QNM) theory, which has experienced substantial advancements over the past decade and has now reached a level of maturity that allows its secure application to numerous contemporary electromagnetic challenges in photonics and plasmonics. Electromagnetic QNMs are source-free solutions of Maxwell equations, $\nabla \times \tilde{\mathbf{E}}_m = -i\tilde{\omega}_m\mu_0\tilde{\mathbf{H}}_m$, $\nabla \times \tilde{\mathbf{H}}_m = i\tilde{\omega}_m\boldsymbol{\epsilon}(\tilde{\omega})\tilde{\mathbf{E}}_m$, in which $\tilde{\mathbf{E}}_m$ and $\tilde{\mathbf{H}}_m$ respectively denote the *normalized* electric and magnetic fields [7], $\boldsymbol{\epsilon}$ denotes the possibly-dispersive permittivity tensors. The QNM field exponentially decays in time and $\text{Im}(\tilde{\omega}_m) < 0$ with the $\exp(-i\omega t)$ notation.

Hereafter, we consider non-magnetic materials, with μ_0 denoting the permeability of vacuum. Extending the analysis to magnetic cases is straightforward [7]. We also assume frequency-independent permittivity for simplicity, emphasizing that the distinctions we uncover between the evolution equations are unrelated to dispersion. The EME for resonators composed of Drude-Lorentz materials [5] will be presented after the derivation of the EME equation.

Subsequently, we adopt the QNM theory with a complex-mapping regularization. This approach has produced highly compelling results, particularly in addressing intricate electromagnetic problems such as those involving branch cuts due to the presence of substrates [5]. The concept of QNM regularization with complex mapping originated in quantum mechanics in the late 1970s. In the realm of electromagnetism, the favored mapping employs a complex scaling transformation known as perfectly matched layers (PMLs). This transformation maps the inherently divergent QNMs of open space onto square-integrable regularized QNMs [9]. For an in-depth examination of QNM regularization, including the use of complex mapping, refer to Section 5.3 in [10].

The regularized QNMs exhibit numerous similarities with the normal modes of Hermitian systems. Specifically, they are square-integrable, can undergo normalization, and can be employed to expand the electromagnetic field $\Psi_s(\mathbf{r}, \omega) \exp(-i\omega t)$ scattered by a resonator illuminated by a monochromatic field oscillating at frequency ω

$$\Psi_s(\mathbf{r}, \omega) = \sum_m \alpha_m(\omega) \tilde{\Psi}_m(\mathbf{r}), \quad (2)$$

where α_m is the complex-valued excitation coefficient of the m^{th} QNM. Throughout the manuscript, Ψ denotes a bivector formed by electric and magnetic fields, for instance $\tilde{\Psi}_m = [\tilde{\mathbf{E}}_m, \tilde{\mathbf{H}}_m]$.

The extension of Eq. (2) encompasses not only QNMs that are unaffected by the PML mapping but also an infinite set of "numerical" eigenvectors. These eigenvectors are computed as source-free solutions of Maxwell equations within the mapped space. Utilizing this expanded basis, highly accurate reconstructions of the field scattered by the resonator have been achieved, even for complex geometries such as resonators with dispersive materials positioned on substrates. Accurate reconstructions have been reported in both spectral [10,11-16] or temporal [5,11] domains.

Differing from the overcompleteness arguments applicable that are relevant to expansions exclusively involving QNMs and resonator geometries in free space, there exists a *unique* expression for the excitation coefficient α_m in the case of nondispersive materials [5]

$$\alpha_m(\omega) = \frac{\omega}{\tilde{\omega}_m - \omega} \int_{V_r} \Delta\boldsymbol{\epsilon}(\mathbf{r}) \mathbf{E}_b(\mathbf{r}, \omega) \cdot \tilde{\mathbf{E}}_m d^3\mathbf{r}. \quad (3)$$

Except for the pole prefactor, α_m essentially represents an overlap integral between the QNM (or numerical modes) and the background field $\Psi_b = [\mathbf{E}_b, \mathbf{H}_b]$ in the absence of resonator. $\Delta\boldsymbol{\epsilon}(\mathbf{r})$ specifies the permittivity variation used for the scattered-field formulation, given by $\Delta\boldsymbol{\epsilon}(\mathbf{r}) = \boldsymbol{\epsilon}_R(\mathbf{r}) - \boldsymbol{\epsilon}_b(\mathbf{r})$, where $\boldsymbol{\epsilon}_R(\mathbf{r})$ and $\boldsymbol{\epsilon}_b(\mathbf{r})$ denote the permittivities of the resonator and the background, respectively. $\Delta\boldsymbol{\epsilon}(\mathbf{r}) \neq 0$ within a compact volume V_r that defines the resonator in the scattered-field formulation.

Unlike other rigorous methods featuring a finite number of QNMs and a background term [17,18], the intrinsic strength of the regularization approach for theoretical works – like the present one – lies in providing a cohesive mathematical framework. In this framework, all eigenstates, QNMs or numerical modes, are treated identically. Owing to the analytical ω -dependence of the excitation coefficient, the resonator response to any incident driving wavepacket can be analytically calculated using a spectral decomposition, summing over all distinct frequencies. Subsequently, the field $\Psi_S(\mathbf{r}, t)$ scattered by the resonator illuminated by a wavepacket can be expressed as a sum of contributions from QNMs and numerical modes [7]

$$\Psi_S(\mathbf{r}, t) = \text{Re}(\sum_m \beta_m(t) \tilde{\Psi}_m(\mathbf{r})), \quad (4)$$

$$\text{with } \beta_m(t) = \int_{-\infty}^{\infty} \alpha_m(\omega) \exp(-i\omega t) d\omega.$$

Using a spectral decomposition of the incident wavepacket, $\mathbf{E}_b(\mathbf{r}, \omega) = (2\pi)^{-1} \int_{-\infty}^{\infty} \tilde{\mathbf{E}}_b(t, \omega) \exp(i\omega t) dt$, and replacing $\alpha_m(\omega)$ with Eq. (3), we get

$$\beta_m(t) = (2\pi)^{-1} \int_{-\infty}^{\infty} \int_{-\infty}^{\infty} \frac{\omega}{(\tilde{\omega}_m - \omega)} O_m(t') \exp(i\omega(t' - t)) d\omega dt'. \quad (5)$$

Here the overlap is now defined as $O_m(t') = \int_{V_r} \Delta\boldsymbol{\epsilon}(\mathbf{r}) \mathbf{E}_b(\mathbf{r}, t') \cdot \tilde{\mathbf{E}}_m d^3\mathbf{r}$.

Hereafter, the EME equation is directly derived from Eq. (5) utilizing complex analysis, with a particular emphasis on Cauchy's integral theorem.

For dispersive PMLs characterized by a complex scaling factor inversely proportional to the frequency, causality is preserved, and all eigenfrequencies of the regularized problem are situated in the lower half of the complex plane. As a result, all temporal excitation coefficients $\beta_m(t)$ can be analytically computed utilizing contour integration and the Cauchy integral formula for the pole $\tilde{\omega}_m$.

We recast Eq. (5) in three terms

$$\beta_m(t) = \int_{-\infty}^{t-\epsilon} \dots + \int_{t-\epsilon}^{t+\epsilon} \dots + \int_{t+\epsilon}^{\infty} \dots = A + B + C, \quad (6)$$

where the three integrands are strictly identical to that in Eq. (5) and ϵ is a small quantity. We will consider the limit $\epsilon \rightarrow 0$ later on.

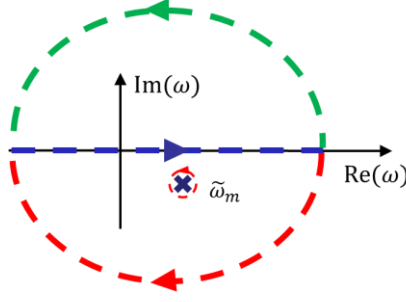


Fig. 1 The two trajectories (red and green arcs) of the complex frequency plane used in the derivation of the EME equation.

Let us first consider the last term, C . To compute the integral, we utilize the upper-plane green arc. Since $\exp(i\omega(t' - t))$ vanishes as $\text{Im}(\omega) \rightarrow \infty$ and there is no pole in the upper plane, we conclude that C equals 0.

Now, let us focus on term A . In this case, the integral is null on the red arc, and the frequency integral is equal to the residue, $2\pi i \tilde{\omega}_m O_m(t') \exp(i\tilde{\omega}_m(t' - t))$. Taking the limit $\epsilon \rightarrow 0$, we find $A = i\tilde{\omega}_m \int_{-\infty}^t O_m(t') \exp(i\tilde{\omega}_m(t' - t)) dt'$.

For term B , we use the equality $\frac{\omega}{(\tilde{\omega}_m - \omega)} = \frac{\tilde{\omega}_m}{(\tilde{\omega}_m - \omega)} - 1$ and obtain $B = B_1 + B_2$, with $B_2 = -\int_{t-\epsilon}^{t+\epsilon} \delta(t' - t) O_m(t') dt' = -O_m(t)$. To demonstrate that B_1 is null, we cast $B_1 = (2\pi)^{-1} \int_{t-\epsilon}^{t+\epsilon} \int_{-\infty}^{\infty} \frac{\tilde{\omega}_m}{(\tilde{\omega}_m - \omega)} O_m(t') \exp(i\omega(t' - t)) d\omega dt'$ into two parts, $B_1 = B_1' + B_1'' = \int_{t-\epsilon}^t \dots + \int_t^{t+\epsilon} \dots$. For B_1' , $t' - t \leq 0$ and the residue theorem applied with the red arc gives us $B_1' = i\tilde{\omega}_m \int_{t-\epsilon}^t O_m(t') \exp(i\tilde{\omega}_m(t' - t)) dt' - \int_{red\ arc} \dots$. By parametrizing the arc path with $\omega = a \exp(i\theta)$ with $a \rightarrow \infty$ and $\theta \in [0, -\pi]$, we show that the modulus of the arc integral is bounded by a finite positive number. Thus, taking the limit $\epsilon \rightarrow 0$ in the temporal integral, we obtain $B_1' = 0$. An identical same reasoning holds for B_1'' by considering the green arc. There is no pole contribution and the arc integral being bounded for the same reason, we have $B_1'' = 0$.

Altogether, we have

$$\beta_m(t) = i\tilde{\omega}_m \int_{-\infty}^t O_m(t') \exp(i\tilde{\omega}_m(t' - t)) dt' - O_m(t), \quad (7)$$

and upon applying the derivative with respect to t on both sides of the equation, we obtain the EME equation

$$\frac{d\beta_m(t)}{dt} = -i\tilde{\omega}_m \beta_m(t) - \frac{d}{dt} \langle \mathbf{E}_b(\mathbf{r}, t) | \Delta \boldsymbol{\epsilon}(\mathbf{r}) | \tilde{\mathbf{E}}_m(\mathbf{r}) \rangle, \quad (8)$$

in which, for convenience, we introduce the notation $\langle \mathbf{E}_b | \mathbf{X} | \tilde{\mathbf{E}}_m \rangle = \int_{V_r} \mathbf{X}(\mathbf{r}) \mathbf{E}_b(\mathbf{r}, t) \cdot \tilde{\mathbf{E}}_m(\mathbf{r}) d^3 \mathbf{r}$ in which \mathbf{X} is an arbitrary 3×3 matrix.

We recall that Eq. (8) holds for non-dispersive materials. A similar derivation can be conducted for dispersive materials [5] using the auxiliary-field method [19,20], with an analytical expression for the permittivity. For instance, in the case of a resonator with a standard multi-pole Lorentz-Drude permittivities and for a dispersionless background in the volume V_r ($\boldsymbol{\epsilon}_b(\mathbf{r})$ may depend on the frequency for $\mathbf{r} \notin V_r$), it was previously shown [5] that

$$\frac{d\beta_m(t)}{dt} = -i\tilde{\omega}_m \beta_m(t) + i\tilde{\omega}_m \langle \mathbf{E}_b | \boldsymbol{\epsilon}_R(\mathbf{r}, \tilde{\omega}_m) - \boldsymbol{\epsilon}_\infty(\mathbf{r}) | \tilde{\mathbf{E}}_m \rangle - \frac{d}{dt} \langle \mathbf{E}_b | \boldsymbol{\epsilon}_\infty - \boldsymbol{\epsilon}_b(\mathbf{r}) | \tilde{\mathbf{E}}_m \rangle, \quad (9)$$

where $\boldsymbol{\epsilon}_\infty$ denotes the high-frequency permittivity constant of the resonator.

Equations (8) or (9) share similarities with the CMT evolution equation. However, differences are apparent. They highlight the incorporation of certain heuristics in CMT which are discussed in the next section.

Further deeper insights into Maxwellian derivation of the CMT, especially regarding outcoupling with ports, can be found in [6].

However, it appears that Eqs. (8) or (9) differ from Eq. (45) in [6], particularly with regard to the final term that incorporates the temporal derivative of the incident electric field $\mathbf{E}_b(\mathbf{r}, t)$. Also, the following discussion on when the CMT evolution equation differs from that in [6].

3. Discussion

We observe three primary distinctions between the EME equation and the classical CMT evolution equation:

- In the CMT, the squared absolute value of the modal excitation coefficient, $|a_m|^2$, signifies the energy stored in the mode m of the resonator. The energy stored in QNMs lacks meaning in a non-Hermitian context: the mode energy is not square integrable since the QNM fields exponentially diverge outside the resonator, see related discussions on the quality factor or the mode volume in [7].
- The second difference, unrelated to hermiticity, arises from the CMT assumption that the mode excitation by the wavepacket occurs *locally*. The local excitation approximation assumes that s_+ is proportional to the wavepacket electric field $\mathbf{E}_{inc}(\mathbf{r}_0, t)$ at an arbitrary point \mathbf{r}_0 typically chosen inside the resonator volume. In contrast, the QNM approach predicts a nonlocal excitation that spans the entire resonator volume through a spatial convolution of the wavepacket and QNM fields. Only in scenarios where the resonator is deep subwavelength, e.g. lump element circuits, does $O_m(t)$ become directly proportional to the incident wavepacket.
- The third difference arises from a driving force proportional to the derivative of the incident field in Eqs. (8) or (9). We do not precisely know the physical origin of this term. Nevertheless, we note that it implies that the excitation coefficient β responds instantaneously to the driving field, as observed with the last term in Eq. (7). We further note that this term is absent in the advanced formulation of Eq. (9) when dispersive materials are considered, specifically for $\epsilon_\infty = \epsilon_b$. For most materials, the high-frequency dielectric constant is anticipated to be approximately 1, indicating that materials behaves as if they were transparent or non-polarizable at high frequency. We have verified that, with the inclusion of background permittivity dispersion, this term vanishes for $\epsilon_R(\omega \rightarrow \infty) = \epsilon_b(\omega \rightarrow \infty) \approx 1$. Nonetheless, it is essential to highlight that the derivative term should be considered in usual simplified models assuming non-dispersive dielectrics.

We now examine under which conditions the CMT evolution equation (1) can yield accurate predictions, in agreement with those provided by the EME equation. We will employ two approximations commonly encountered in experiments. The first approximation arises from the fact that incident wavepackets can often be described as the product of a slowly-varying envelope function, denoted as $H(t)$, and a fast carrier signal, $\exp(-i\omega t)$. Thus, the electric field of the incident wavepacket can be expressed as $\mathbf{E}_b = \mathbf{E}_0 H\left(t - \mathbf{r} \cdot \frac{\mathbf{u}}{c}\right) \exp\left(-i\omega\left(t - \mathbf{r} \cdot \frac{\mathbf{u}}{c}\right)\right)$, \mathbf{u} being a unitary vector parallel to the incident wavevector. Under the slowly-varying envelop approximation, $\frac{d}{dt} \langle \mathbf{E}_b | \Delta \epsilon(\mathbf{r}) | \tilde{\mathbf{E}}_m \rangle$ in Eq. (8) approximately becomes $-i\omega \langle \mathbf{E}_b | \Delta \epsilon(\mathbf{r}) | \tilde{\mathbf{E}}_m \rangle$. Another commonly encountered scenario involves resonators characterized by subwavelength dimensions, such as RLC lump-element circuits. In these instances, it is reasonable to assume that the incident wavepacket uniformly occupies the resonator volume, and the overlap integrals $\langle \mathbf{E}_b | \Delta \epsilon(\mathbf{r}_0) | \tilde{\mathbf{E}}_m \rangle$ reduces to $\langle \mathbf{E}_b(\mathbf{r}_0, t) | \Delta \epsilon(\mathbf{r}) | \tilde{\mathbf{E}}_m \rangle$, \mathbf{r}_0 being the ‘center of mass’ of the resonator.

By utilizing these two approximations, we effectively achieve a primary goal of this study: deriving an analytical expression for the coupling constant outlined in Eq. (1)

$$\langle \kappa_m^* | s_+ \rangle \equiv i\omega \langle \tilde{\mathbf{E}}_m | \Delta \epsilon(\mathbf{r}_0) | \mathbf{E}_b(\mathbf{r}_0, t) \rangle, \quad (10)$$

where $\tilde{\mathbf{E}}_m$ represents the electric field of the *normalized* QNM and ω is the carrier frequency.

The prevalence of slowly-varying envelopes and subwavelength resonators in many applications, coupled with the reluctance to quantitatively compare CMT predictions with experimental data or the absence of a QNM framework in the recent past, may explain why earlier experiments did not

reveal any anomalies in CMT predictions. We now provide a qualitative assessment of the impact of these two approximations.

Equation (9) has been quantitatively tested for a gold bowtie antenna illuminated by a Gaussian pulse with a central frequency in the visible range, see Fig. 2 in [5]. Given this verification, we focus on offering a qualitative illustration, discussing significant trends. We have first assessed the validity of Eq. (10) for Gaussian envelopes and subwavelength resonators. Given the gentle variations of Gaussian envelopes, a very good agreement has been achieved, even for short pulses spanning 20 cycles.

In Fig. 2, we compare the predictions obtained with the EME equation (cyan curve) and Eq. (10) (red curve), for increasing resonator sizes (s) and two pulse shapes shown in grey. The results are obtained for an excitation with a complex frequency $\omega = 1 - 0.05i : \mathbf{E}_0 S(u) \exp(-i\omega u)$, where $u = t - (x - x_c)/c$, $c = 1$, and $S(u) = (1 + e^{-\rho u})^{-1}$ is the sigmoid function, approaching a Heaviside function for large values of ρ . Two values of ρ are considered: $\rho = 0.1$ in Fig. 2a and $\rho = 1$ in Figs. 2b and 2c. The pulses are assumed to hint the mass center x_c of the resonator at time $t = 0$. Their shapes are shown with grey curves. For the simulation, the electric field of the QNM is chosen to be spatially uniform in the volume V_r .

Consistently with the study with Gaussian pulses, we find a perfect agreement for subwavelength resonators ($s = 0.1\lambda$) and gentle wavefront ($\rho = 0.1$), see Fig. 2a. A noteworthy observation is that Eq. (10) remains approximately applicable even when the resonator size is half a wavelength. Indeed, the precision of Eq. (10) can be significantly enhanced by introducing a suitably fitted scaling prefactor. For instance, we have verified that a rescaled version of the red curve in panel (b) aligns perfectly with the EME equation prediction. It is important to note, however, that such rescaling loses its effectiveness for larger resonator sizes, as evidenced by its inability to predict the double peak response of the EME equation in panel (c).

Despite the heuristic nature of its derivation, the classical CMT equation, Eq. (1), with a fitted coupling constant, proves to be a robust model. This robustness arises from a fundamental mathematical property of the exponential function: its preservation under differentiation and integration. This property establishes a proportional relationship between the carrier signal and the derivative term and the nonlocal overlap of the EME equation.

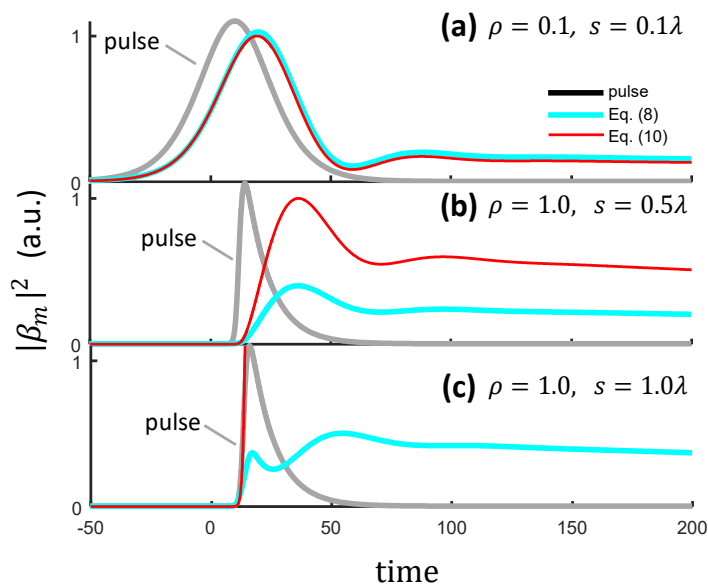


Fig. 2 Comparative analysis of the predictions obtained with the EME equation (8) (cyan curves) and the CMT evolution equation (1) with the analytical coupling constant given by Eq. (10) (red curve). We consider several resonator sizes ($s = 0.1, 0.5$ and 1λ) and pulse shapes ($\rho = 0.1$ and 1) depicted with grey curves for clarity reasons. Panels (a), (b), and (c) depict scenarios with gentle sigmoid and deep subwavelength resonator size (high accuracy for Eq. (10)), steep sigmoid and subwavelength size (limited accuracy for Eq. (10)), and steep sigmoid and wavelength-scale resonator (significant inaccuracy and failure for Eq. (10)). Key parameters are $\omega = 1 - 0.05i$, $\tilde{\omega}_m = 1.1 - 0.0025i$. The resonator sizes are given in units of the wavelength ($\lambda = 2\pi c/\text{Re}(\omega)$).

Acknowledgements

PL acknowledges Sander Mann and Andrea Alù for helpful discussions during his visit at CUNY in November 2023. The authors acknowledge Wei Yan for his initial important contribution of the derivation of Eq. (9). PL acknowledges financial supports from the WHEEL (ANR-22CE24-0012-03) Project and the European Research Council Advanced grant (Project UNSEEN No. 101097856).

References

1. H. A. Haus, *Waves and Fields in Optoelectronics*, 1st ed. (Prentice-Hall, 1984).
2. H. A. Haus and W. Huang, "Coupled-mode theory", *Proc. IEEE* **79**, 1505 (1991).
3. W. Shu, Z. Wang, and S. Fan, "Temporal coupled-mode theory and the presence of non-orthogonal modes in lossless multimode cavities", *IEEE J. Quant. Electron.* **40**, 1511 (2004).
4. S. Fan, W. Suh, and J. D. Joannopoulos, "Temporal coupled mode theory for Fano resonances in optical resonators", *J. Opt. Soc. Am. A* **20**, 569 (2003).
5. W. Yan, R. Faggiani, and P. Lalanne, "Rigorous modal analysis of plasmonic nanoresonators", *Phys. Rev. B* **97**, 205422 (2018).
6. H. Zhang and O. D. Miller, "Quasinormal Coupled Mode Theory", arXiv preprint, arXiv:2010.08650.
7. P. Lalanne, W. Yan, K. Vynck, C. Sauvan, and J.-P. Hugonin, "Light interaction with photonic and plasmonic resonances", *Laser Photonics Rev.* **12**, 1700113 (2018).
8. M. Zworski, *Mathematical study of scattering resonances*, *Bull. Math. Sci.* **7**, 1-85 (2017).
9. C. Sauvan, J.P. Hugonin, I.S. Maksymov, and P. Lalanne, "Theory of the spontaneous optical emission of nanosize photonic and plasmon resonators", *Phys. Rev. Lett* **110**, 237401 (2013).
10. C. Sauvan, T. Wu, R. Zarouf, E. A. Muljarov, and P. Lalanne, "Normalization, orthogonality, and completeness of quasinormal modes of open systems: the case of electromagnetism", *Opt. Express* **30**, 6846-6885 (2022).
11. F. Olyslager, "Discretization of continuous spectra based on perfectly matched layers", *SIAM J. Appl. Math.* **64**, 1408-1433 (2004).
12. B. Vial, A. Nicolet, F. Zolla, M. Commandré, "Quasimodal expansion of electromagnetic fields in open two-dimensional structures", *Phys. Rev. A* **89**, 023829 (2014).
13. J. Zimmerling, L. Wei, P. Urbach, and R. Remis, "A Lanczos model-order reduction technique to efficiently simulate electromagnetic wave propagation in dispersive media", *J. Comput. Phys.* **315**, 348-362 (2016).
14. F. Zolla, A. Nicolet, G. Demésy, "Photonics in highly dispersive media: the exact modal expansion", *Opt. Lett.* **43**, 5813-5816 (2018).
15. A. Gras, P. Lalanne, M. Duruflé, "Non-uniqueness of the Quasinormal Mode Expansion of Electromagnetic Lorentz Dispersive Materials", *J. Opt. Soc. Am. A* **37**, 1219-28 (2020).
16. X. Ming, "Quasinormal Mode Expansion Method for Resonators with Partial-fraction Material Dispersion", arXiv preprint, arXiv:2312.11048
17. L. Zschiedrich, F. Binkowski, N. Nikolay, O. Benson, G. Kewes, S. Burger, "Riesz-projection-based theory of light-matter interaction in dispersive nanoresonators", *Phys. Rev. A* **98**, 043806 (2018).
18. T. Wu, D. Arrivault, W. Yan, P. Lalanne, "Modal analysis of electromagnetic resonators: user guide for the MAN program", *Comput. Phys. Commun.* **284**, 108627 (2023).
19. R. M. Joseph, S. C. Hagness, and A. Taflove, "Direct time integration of Maxwell's equations in linear dispersive media with absorption for scattering and propagation of femtosecond electromagnetic pulses", *Opt. Lett.* **16**, 1412 (1991).
20. A. Raman and S. Fan, "Photonic Band Structure of Dispersive Metamaterials Formulated as a Hermitian Eigenvalue Problem", *Phys. Rev. Lett.* **104**, 087401 (2010).